Check for updates

ADVANCING EARTH AND SPACE SCIENCES

JGR Solid Earth

RESEARCH ARTICLE
10.1029/2023JB028606

Key Points:

- Negative field-dependence of magnetic susceptibility is poorly understood and occurs in rocks near the basement unconformity of NE Oklahoma
- This behavior is due to low-field magnetic saturation of an unknown magnetic carrier with a magnetic ordering temperature near 80°C
- The carrier is associated with frequency-dependence of susceptibility and fluid alteration and may complicate environmental studies

Supporting Information:

Supporting Information may be found in the online version of this article.

Correspondence to:
M. Hamilton,
matt-hamilton@utulsa.edu

Citation:
Hamilton, M., Jackson, M., Chadima, M., Egli, R., & Elmore, R. D. (2024). Strongly negative low-field variation of magnetic susceptibility: Rock magnetic character of the basement-cover interface of northeastern Oklahoma. *Journal of Geophysical Research: Solid Earth*, *129*, e2023JB028606. https://doi.org/10.1029/2023JB028606

Received 20 DEC 2023
Accepted 21 JUL 2024

Author Contributions:
Conceptualization: Matt Hamilton
Data curation: Matt Hamilton, Mike Jackson, Martin Chadima
Formal analysis: Matt Hamilton, Mike Jackson, Ramon Egli
Funding acquisition: R. Douglas Elmore
Investigation: Matt Hamilton, Mike Jackson, Martin Chadima, Ramon Egli
Methodology: Matt Hamilton, Mike Jackson, Martin Chadima
Resources: Matt Hamilton, Mike Jackson, Martin Chadima, R. Douglas Elmore
Software: Mike Jackson, Martin Chadima
Supervision: R. Douglas Elmore
Validation: Martin Chadima
Visualization: Matt Hamilton, Martin Chadima, Ramon Egli
Writing – original draft: Matt Hamilton

© 2024. American Geophysical Union. All Rights Reserved.

Strongly Negative Low-Field Variation of Magnetic Susceptibility: Rock Magnetic Character of the Basement-Cover Interface of Northeastern Oklahoma

Matt Hamilton[1], Mike Jackson[2], Martin Chadima[3,4], Ramon Egli[5], and R. Douglas Elmore[6]

[1]Department of Geosciences, University of Tulsa, Tulsa, OK, USA, [2]Institute for Rock Magnetism, University of Minnesota, Minneapolis, MN, USA, [3]AGICO, Inc, Brno, Czech Republic, [4]Institute of Geology of the Czech Academy of Sciences, Prague, Czech Republic, [5]Department of Geophysics and Conrad Observatory, GeoSphere Austria, Vienna, Austria, [6]School of Geosciences, University of Oklahoma, Norman, OK, USA

Abstract Some rock and soil samples exhibit significant loss of magnetic susceptibility (χ) with increasing applied field amplitude even at relatively low (10–100s of A/m) fields, a behavior which remains unexplained. Exceptionally strong negative field-dependence of susceptibility (χ_{HD}) is present in sandstones and altered intermediate-felsic igneous rocks in several cores from the northeastern Oklahoma subsurface. These same rocks also show elevated frequency-dependence of susceptibility (χ_{FD}), with reasonable correlation of χ_{HD} to χ_{FD}, and frequency-dependent χ_{HD}. Results from multiple characterization methods indicate that strongly negative χ_{HD} in these rocks is linked to a yet-unidentified phase which begins the approach to magnetic saturation in low fields (<1 mT/800 A/m), shows elevated χ_{FD} to low temperatures, is unstable at high temperatures, possesses significant anisotropy of magnetic susceptibility, and becomes paramagnetic above ~83°C. Clear associations with fluid alteration features indicate that this material may be highly relevant to rock alteration, diagenetic, and environmental studies.

Plain Language Summary Magnetic susceptibility is usually measured using weak magnetic fields, and in many geological materials the value depends on the strength of the field used. In the low-field range, this usually results in slightly higher susceptibility values as field strength increases. In some rocks and soils, however, susceptibility decreases with increasing applied field, which has not been explained. The lowermost sandstones and uppermost igneous rocks in the northeastern Oklahoma subsurface have been found to provide prominent examples of this "negative field-dependence" of susceptibility. When susceptibility of the same rocks is measured using an alternating-current field, the results are also highly dependent on the frequency of that field. The strength of these behaviors is correlated, and both are found to be associated with a yet-unidentified magnetization carrier with an apparent Curie temperature of ~83°C. Through direct-current measurements, it is apparent that the negative field-dependence is due to this mineral approaching magnetic saturation at unusually low fields relative to most natural materials. The magnetic behavior is associated with other evidence of water-rock interaction, which may prove to be a useful indicator of chemical conditions of alteration, diagenesis, and weathering.

1. Introduction

The magnetic susceptibility (k if volume-normalized, or χ if mass-normalized) of rocks and soils is commonly measured using low-field (tens to hundreds of A/m) alternating current (AC) instruments which operate at frequencies of several hundred to several thousand Hz. While the susceptibilities of diamagnetic and paramagnetic materials are in phase with the applied AC field and independent of its amplitude, the measured susceptibilities of ferromagnetic *sensu lato* materials may vary significantly depending on the amplitude (χ_{HD}) and frequency (χ_{FD}) of the measuring field (e.g., Worm, 1991, 1998). They may additionally have a susceptibility component that is out of phase with the measuring field (sometimes referred to as out-of-phase, imaginary, or quadrature susceptibility) which is also typically dependent on frequency and/or field strength (Jackson, 2004). Variations of in-phase and out-of-phase susceptibility with changes in frequency and amplitude may provide information on the composition and grain size of the ferromagnetic *s.l.* mineral fraction in natural materials.

The magnetization (M) of diamagnetic, paramagnetic, and (at sufficiently low fields) ferromagnetic *s.l.* materials follows the linear relationship $M = kH$, where k is susceptibility and H is the applied field. For some ferromagnetic

Writing – review & editing: Matt Hamilton, Mike Jackson, Martin Chadima, Ramon Egli, R. Douglas Elmore

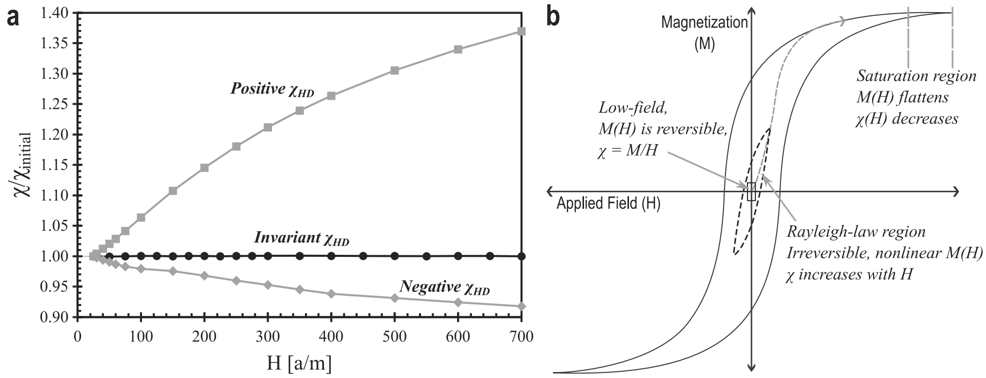

Figure 1. (a) Examples of field-dependence of magnetic susceptibility (χHD). Positive χHD sample is a basalt, invariant sample is jarosite, both samples from University of Oklahoma teaching collections. Negative χHD sample is a sandstone from this study. (b) Schematic magnetic hysteresis diagram after Borradaile et al. (2008), showing relative field values at which different χ(H) behaviors may be expected.

s.l. minerals, the magnetization is linear (and therefore susceptibility is constant) in the low-field range. For others, particularly multidomain state particles, the magnetization follows the Rayleigh Law $M = k_i H + \alpha H^2$, where k_i is the initial susceptibility, and α is the Rayleigh coefficient (Hrouda et al., 2006). The magnetic susceptibility is then dependent on the field: $k = \mathrm{d}M/\mathrm{d}H = k_i + 2\alpha H$, where $\alpha \geq 0$. Measurements at varying field amplitudes have shown substantial magnetic susceptibility increases in geological materials, including pyrrhotite (Worm, 1991), titanomagnetite (Jackson et al., 1998), and hematite (Guerrero-Suarez & Martín-Hernández, 2012; Hrouda, 2002), though these do not always follow the linear Rayleigh relation. Consequently, field-dependent susceptibility variation (Figure 1) has found application in rocks as a magnetic mineralogy indicator (Hrouda et al., 2006; Vahle & Kontny, 2005). Some environmental and geological materials however have a *negative* field-dependence, that is, they decrease in susceptibility with increasing applied field (Chlupáčová et al., 2010; Hrouda et al., 2006). At high fields (tens of thousands of A/m or higher) this behavior results from the saturation of ferro- or ferrimagnetic minerals (Borradaile et al., 2008) but its presence at low fields (tens to hundreds of A/m) has not been explained to date.

This study documents significant negative field-dependence of susceptibility (χ_{HD}) in specimens from the lowermost clastic sediments and uppermost igneous "basement" rocks in the northeastern Oklahoma subsurface. Preliminary study of the subsurface nonconformity between Mesoproterozoic trachyte and (presumably) Cambrian sandstone in the Amoco SHADS 4 drill core found that the sandstone and uppermost trachyte near the unconformity lose a significant amount (up to ∼10%) of their susceptibility as the measuring field strength increases from 5 to 700 A/m (Hamilton et al., 2018). This study extends the investigation to several other cores in the region (Figure 2) and includes more detailed rock magnetic analyses in order to better understand this unusual behavior.

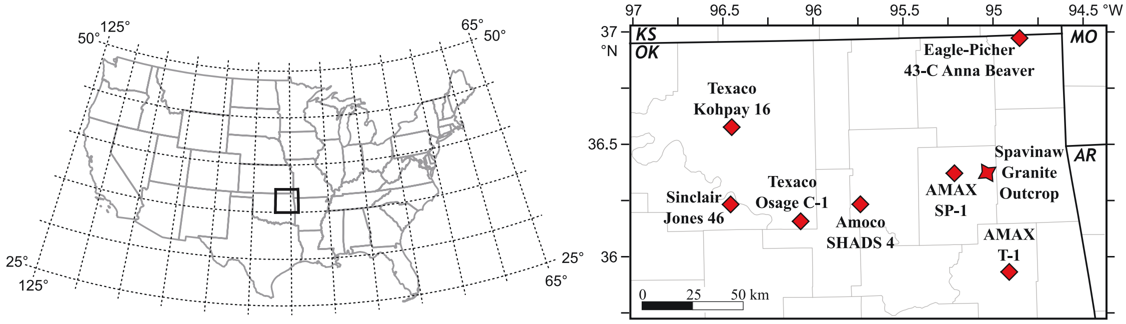

Figure 2. Map locations of general study area and individual cores.

21699356, 2024, 8, Downloaded from https://agupubs.onlinelibrary.wiley.com/doi/10.1029/2023JB028606 by University Of Minnesota Lib, Wiley Online Library on [13/11/2024]. See the Terms and Conditions (https://onlinelibrary.wiley.com/terms-and-conditions) on Wiley Online Library for rules of use; OA articles are governed by the applicable Creative Commons License

Table 1
Cores, Depth Ranges and Lithologies

Core name	Abbr.	# Samples	# Bulk specimens	Depth range (m)	Lithologies
Amoco SHADS4	S4	37	132	882.7–1,046.1	Sandstone, Trachyte
AMAX SP-1	SP1	14	16	531.7–543.2	Sandstone, Granite
AMAX T-1	T1	7	7	415.7–436.5	Sandstone, Trachydacite
Eagle-Picher 43-C Anna Beaver	43C	4	4	492.9–499.3	Sandstone, Granite
Sinclair Louisa M. Jones 46	SJ46	7	23	893.3–897.0	Rhyolite
Texaco Kohpay 16	TK16	1	3	866.7	Microgranite
Texaco Osage C1	OC	3	7	1,123.2–1,124.7	Rhyolite

2. Materials and Methods

2.1. Materials and Geological Context

Rock samples in this study come from seven subsurface cores of the upper igneous basement and immediately overlying sediments in northeastern Oklahoma (Figure 2), all of which are owned and housed by the Oklahoma Geological Survey at the Oklahoma Petroleum Information Center (OPIC). Samples were collected as either small slabs or as azimuthally-unoriented core plugs, with many samples large enough to be trimmed into several smaller specimens. A total of 192 bulk specimens from 73 independent samples are included in this study (Table 1). Specimens from 13 of those samples were further subsampled for detailed rock magnetic investigation (Table 2).

The igneous rocks of this area are comprised of mostly granites and rhyolites with consistent U-Pb zircon ages of approximately 1,370 Ma (Bickford et al., 2015). Rb-Sr age determinations range from 50 to nearly 200 million years younger than the zircon dates (Denison, 1981) due to alteration, which has also been documented petrographically (Denison, 1981; Hamilton et al., 2021). Clastic sediments (where present) consist mainly of medium to coarse arkosic sandstones that appear to be derived from the underlying basement, are overlain by early Ordovician carbonates, and are not well-dated but are generally assumed to be of upper Cambrian age (Derby et al., 1991; McCracken, 1964). The overlying carbonates are not studied here.

Igneous rocks in this study are mostly pink to red in appearance, although in some intervals secondary alteration has turned them a gray color. Chlorite is common, and traces of pyrite and/or jarosite have been found in some thin sections (Hamilton et al., 2021). Sedimentary samples are mostly yellowish, gray, or white arkosic sandstones with variable amounts of clay minerals and pyrite. The northeasternmost part of the study area lies within the Tri-State Mineral District, which was exploited for lead and zinc sulfides in the early 20th century. While some of the cores were drilled by mining exploration companies prospecting for subsurface ores, none contain substantial metal mineralization beyond minor intervals with up to a few percent pyrite. Other cores come from oil and gas wells as much as ~150 km away from the mineral district. Specimens from the lone igneous outcrop in the area (the Spavinaw Granite) did not exhibit negative field-dependence or detectable frequency-dependence of susceptibility.

Table 2
Samples Used in Detailed Rock Magnetic Analysis

Sample name	Depth (m)	Lithology
43C-7	493.8	Highly Altered Granite
OC1-1	1,123.2	Rhyolite
S4-104	918.8	Altered Trachyte
S4-113	917.3	Altered Trachyte/Conglomerate
S4-116	916.8	Altered Trachyte
S4-126	911.7	Sandstone
S4-129	909.3	Sandstone
SJ46-10	896.6	Rhyolite
SJ46-2938	895.5	Rhyolite
SJ46-6	895.2	Rhyolite
SP1-5	532.4	Altered Granite
T1-6	435.6	Altered Rhyolite
TK16-12	866.7	Microgranite

2.2. Methods

Room-temperature bulk magnetic susceptibility measurements were made using an AGICO MFK1 Kappabridge at the University of Oklahoma; selected specimens were also measured using MFK2 and KLY5 Kappabridges at AGICO, Inc. (Brno, Czech Republic). Field-dependence was measured at a frequency of 976 Hz and peak fields ranging from 5 to 10 A/m to 700 A/m. Field-dependence values are reported as $\chi_{HD}[\%] = 100(\chi_{Hmax} - \chi_{Hmin})/\chi_{Hmin}$ with H_{max} = 700 A/m and H_{min} = 100 A/m, as measurements using field amplitudes below 100 A/m sometimes have increased uncertainty. Frequency-dependence was measured using a peak applied field of 200 A/m

21699356, 2024, 8, Downloaded from https://agupubs.onlinelibrary.wiley.com/doi/10.1029/2023JB028606 by University Of Minnesota Lib, Wiley Online Library on [13/11/2024]. See the Terms and Conditions (https://onlinelibrary.wiley.com/terms-and-conditions) on Wiley Online Library for rules of use; OA articles are governed by the applicable Creative Commons License

21699356, 2024, 8, Downloaded from https://agupubs.onlinelibrary.wiley.com/doi/10.1029/2023JB028606 by University Of Minnesota Lib, Wiley Online Library on [13/11/2024]. See the Terms and Conditions (https://onlinelibrary.wiley.com/terms-and-conditions) on Wiley Online Library for rules of use; OA articles are governed by the applicable Creative Commons License

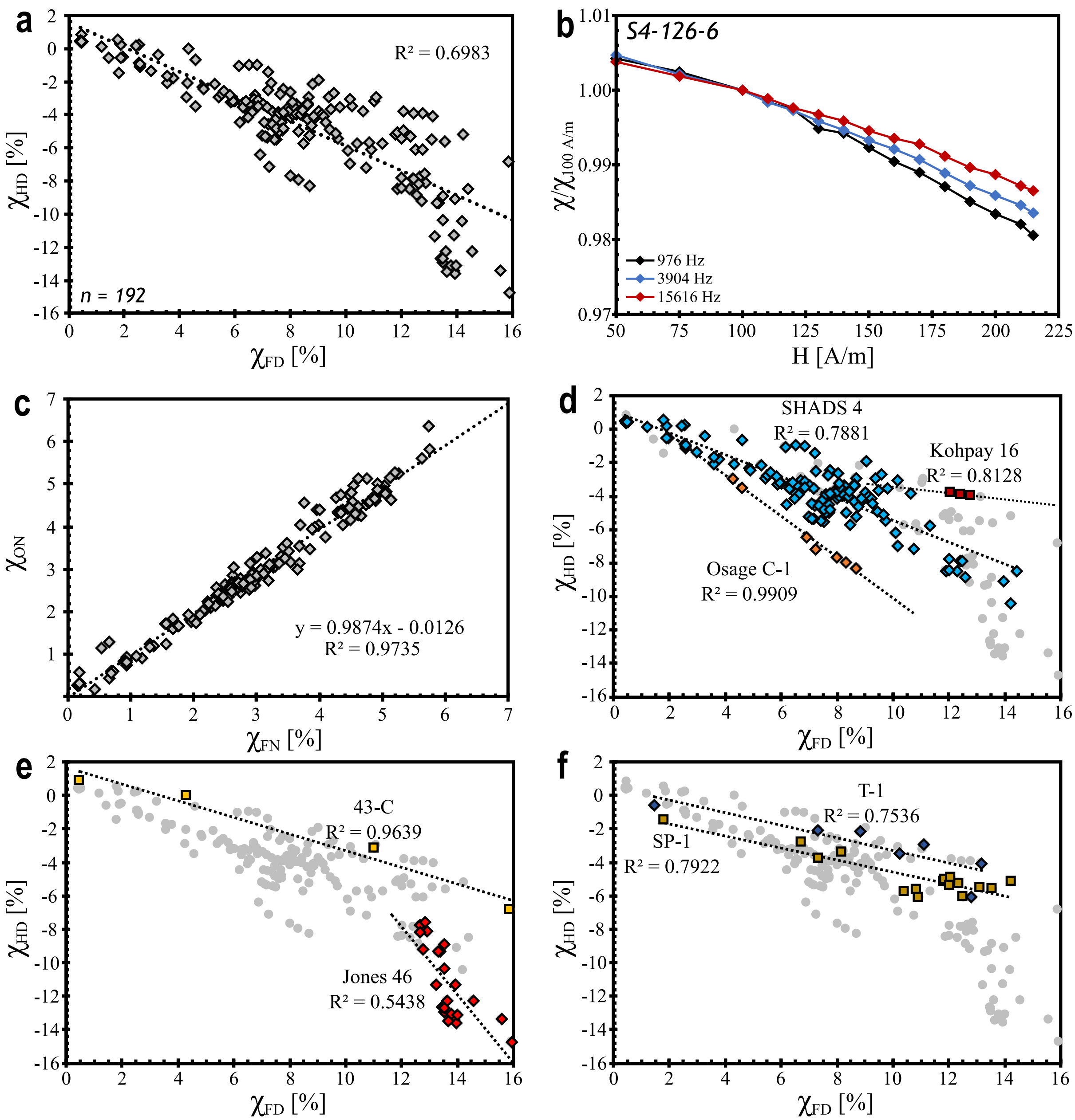

/ 0 & ' 1)7))) 9 7)) ' & 5/' 0:)7))
9) & 8 (1 &)) Ω8 9 5/ 0# 7 7 & ' Ω 1 &
%) 9 7)) Ω 5/)3 0 & Ω8 Ω & 5

/ 25ΑΝ0 1 &) % /: 0 1 & & & & 7
7 &) . /8) 5 2 05

' 1 :) 8 & 1) ') & 8 (1 & &
& 1 & P)58 1 &))
& ') /:)3 05 & 1 & G 5B
(- / 25 (0 1 & & ') & 1 & 1 : 8 1 & 25N &
5 & &) & ' 1 8
') 1 & : 5 &) & 1 & 1 &) : 1 &
Ω8 Z # / : ;5(Μ0) &@
1 & / : 5 Μ0)) 8 25 25 Μ5

21699356, 2024, 8, Downloaded from https://agupubs.onlinelibrary.wiley.com/doi/10.1029/2023JB028606 by University Of Minnesota Lib, Wiley Online Library on [13/11/2024]. See the Terms and Conditions (https://onlinelibrary.wiley.com/terms-and-conditions) on Wiley Online Library for rules of use; OA articles are governed by the applicable Creative Commons License

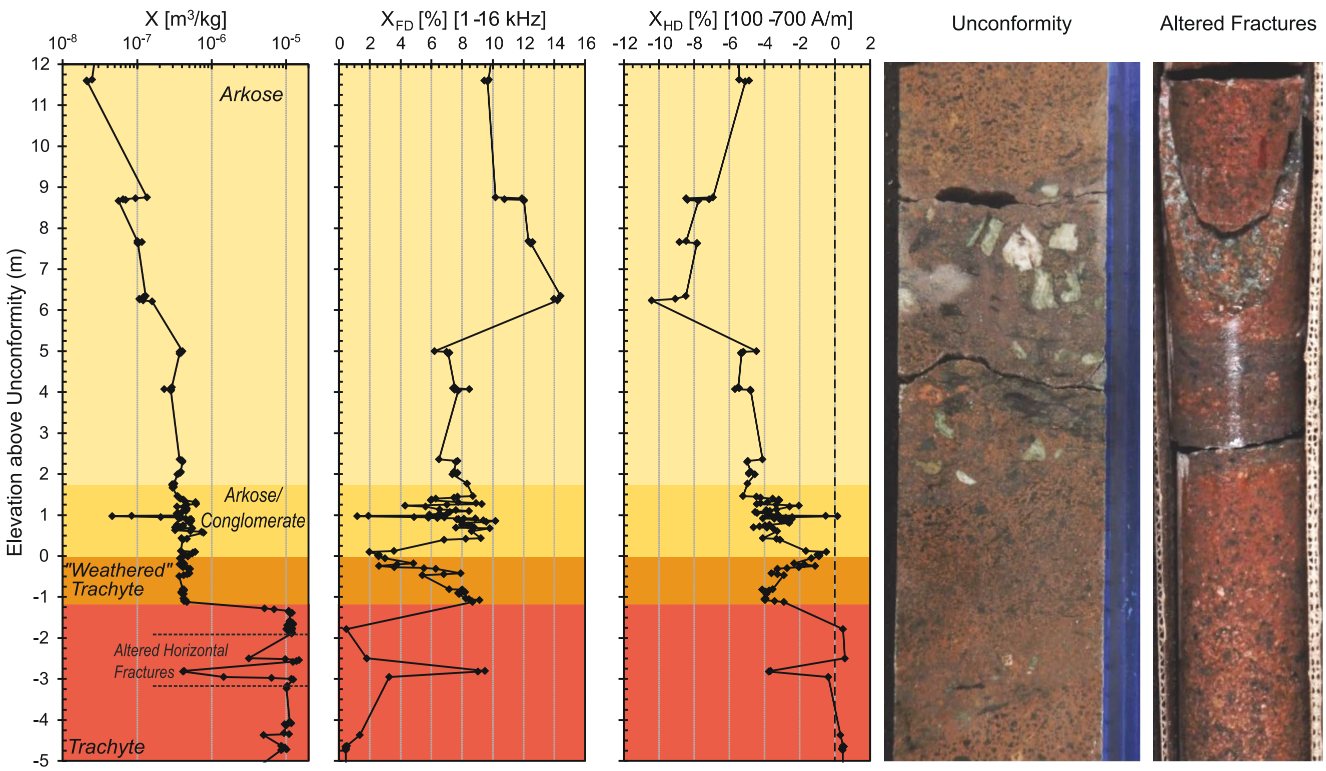

Figure 4. In-phase magnetic susceptibility and its dependence on frequency and field strength near the basement unconformity of the Amoco SHADS 4. Core photographs are of the basement-cover contact and altered fractures.

Altered trachyte samples in the SHADS 4 core with significant χ_{FD} and negative χ_{HD} have notably lower bulk susceptibility values than less-altered specimens, which have negligible χ_{FD} and zero to positive χ_{HD} (Figure 4). The same general relationship is found in other cores also containing igneous rock which does not have elevated χ_{FD} or negative χ_{HD}. Negative χ_{HD} values are strongest in the sandstones, but also appear in highly altered trachyte near the unconformity as well as along some roughly horizontal fractures re-cemented by chlorite and carbonate. Elevated χ_{FD} alongside negative χ_{HD} is also seen in a sheared, highly reddened breccia in trachyte ~100 m below the basement unconformity of the SHADS 4.

3.2. Hysteresis

High-field hysteresis measurements have a range of behaviors (Figure 5). Most samples have low bulk coercivity (B_c), of a few mT to a few tens of mT. Some loops saturate at a few hundred mT (Figures 5a–5c), while others are evidently constricted and do not saturate completely until fields of 1–1.5 T or higher (Figures 5d–5f). Values of σ_{hys} (Fabian, 2003) are weakly to strongly positive for all samples, indicating a tendency toward constricted, "wasp-waisted" shapes. These shapes result from an unusually wide or bimodal distribution of coercivities, as for instance in mixtures of low- and high-coercivity minerals (Tauxe et al., 1996), yielding large B_{cr}/B_c ratios that depart from the M_{rs}/M_s versus B_{cr}/B_c trend of (titano)magnetite (Dunlop, 2002). Samples from the Jones 46 (Figures 5e and 5f) are evidently a mixture of a low-coercivity phase, which is responsible for the large slope of the hysteresis branches near $B = 0$, and a high-coercivity phase that remains unsaturated at applied fields of 2 T. The loop constriction at low coercivities, such as those of SHADS 4 samples (Figure 5a) is more subdued but still present.

Minor hysteresis loop measurements with low maximum fields (up to 1 mT (≈800 A/m)) are noisy but have nearly linear reversible behavior at low fields (≤0.5 mT) (Figure 6). Linear regression of data from samples with appreciable negative χ_{HD} yields lower slopes at higher peak fields. At maximum fields ≥1 mT, nonlinear behavior is visible in $M(H)$ curves for several specimens. These curves shallow at the ends of the field range, which suggests the presence of a phase which approaches saturation within a few mT.

21699356, 2024, 8, Downloaded from https://agupubs.onlinelibrary.wiley.com/doi/10.1029/2023JB028606 by University Of Minnesota Lib, Wiley Online Library on [13/11/2024]. See the Terms and Conditions (https://onlinelibrary.wiley.com/terms-and-conditions) on Wiley Online Library for rules of use; OA articles are governed by the applicable Creative Commons License

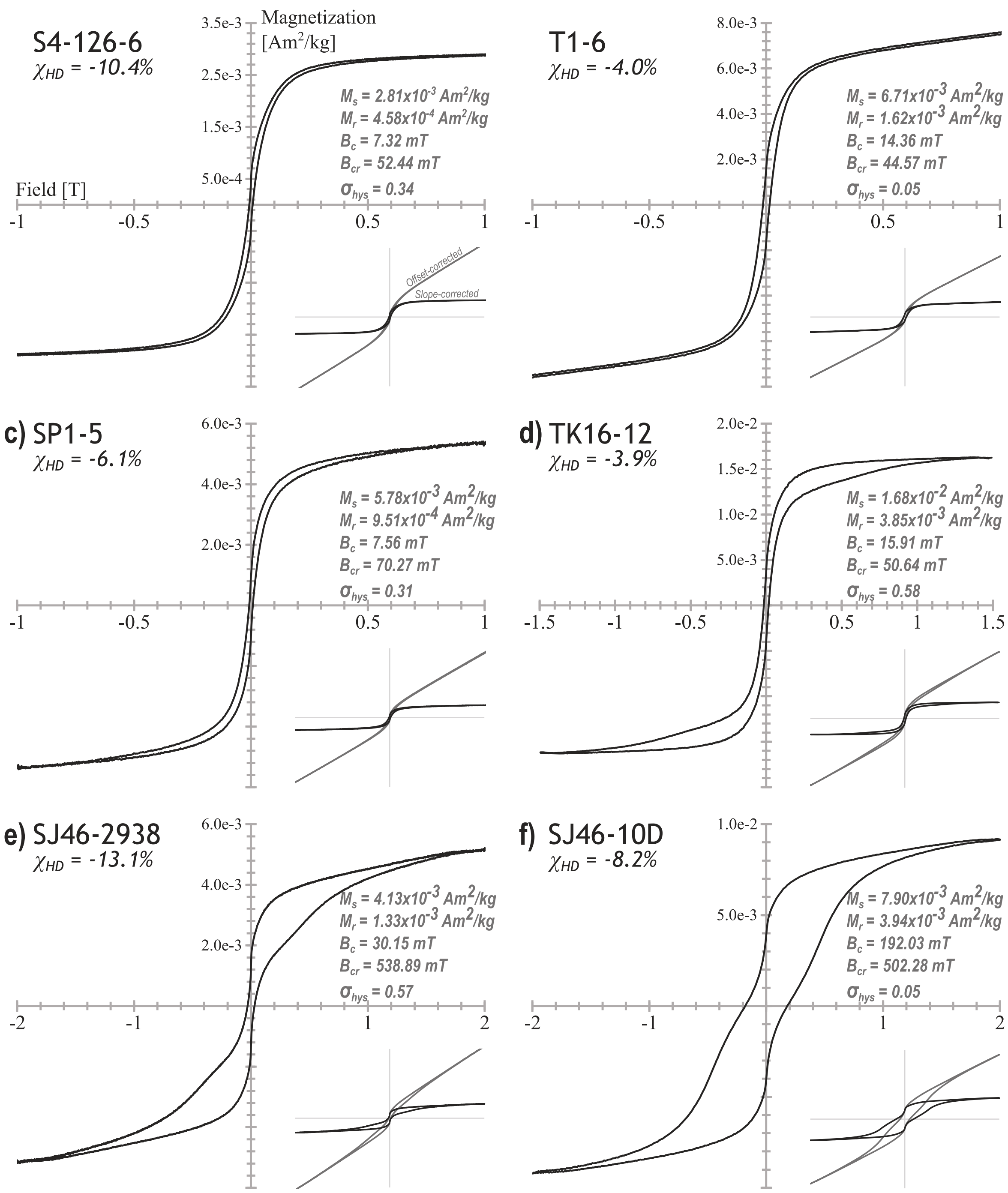

Figure 5. Representative slope-corrected high-field (1–2 T) hysteresis loops of specimens with negative χHD, with a range of coercivities and shapes. Inset plots are of data before and after slope-correction. Sample names begin with abbreviated core names (see Figure 2, Tables 1 and 2).

3.3. Low-Temperature Remanence

Remanence versus temperature curves indicate a variety of carrier minerals, but with inconsistent results (Figure 7). Most specimens have slightly "humped" curves from low-temperature demagnetization (LTD) of room-temperature SIRM (e.g., Figures 7a–7c, 7g, and 7i), a feature linked to oxidized magnetite (Özdemir & Dunlop, 2010). Low-temperature demagnetization curves of SIRM (LTD-RTSIRM) from the Jones 46, Kohpay 16, and SP-1 specimens also have prominent remanence drops near 260 K, consistent with the Morin transition of

21699356, 2024, 8, Downloaded from https://agupubs.onlinelibrary.wiley.com/doi/10.1029/2023JB028606 by University Of Minnesota Lib, Wiley Online Library on [13/11/2024]. See the Terms and Conditions (https://onlinelibrary.wiley.com/terms-and-conditions) on Wiley Online Library for rules of use; OA articles are governed by the applicable Creative Commons License

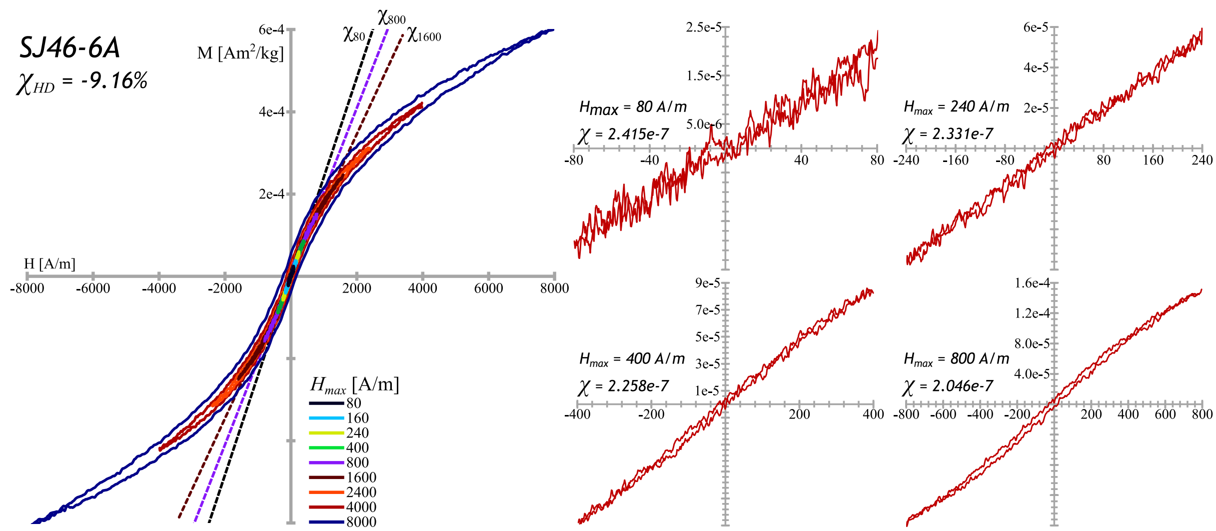

G 1 7) & B(- 7- 5/G 0G 1 7) ; 2 ; 222 4 1 & .)))
& 5/ &0G 1 7)) / ; 22 4 0 1 &) & 1 1 & &) 5# ' ' ; 22 4 5

& / 5 5 [%) 5 22; 0/: N) N) N&05G & & ' 1 & # 7
2M /: N0) & (7# M
/: N05 &) G / # [%) E 2 20)
1 7) A2) 22 / N3 N # 0) .)
: N5

G 1 7 & 1 & & , 1 / 0 / 5 5 # 7
% 5 22- KB E 1 % 2 K 1 % 5 AA; 0 '
' & 5 & & &
/ 5N 5(# 0 ' & A 1 5) 7 /: # 0
& % 7) 7) 1 7 /X: # 7G 0 1
& & & ' 1 & & 5
1 &) G 7)) 7) /: # 0
) X: # G) 1 & & - 2 / # 0 1 & & & X: # .) & : #
/ 5 5 : N) 05 # &) 1 & : # 7X: #) & B (-)
7) ' & (7# 5 & : N)
22 / N # 0 : # 7X: # 1) (22 / N # 0 5 & &
) ' 22 / N # 0 1 ') ' (22 / N # 0 1 & & & &
' 5

: # 7X: # G &) & /: N N N N) N&0 & %) '
%) & 2 K ' 2 &
) , 1 /: N 0 ') 5 &) &
& , 1)) ' & 9 : N N N N& N N
N) N5 & 1 &) 1 7 .)
/ 22 K E) 22205 & (# 7N/: N0 & , 1
) ' : # 7X: # G ') & G 7 1 & & @
) .) 5 & %) ') 8
& .) . 8 5

: & /: N N) N0)) ' &
: #) X: # G & & .
/G 5 22- 05 & ' & & . 1) @
& ' & / & 5 2 0)) % 5 & & &
& . : N) 1 & & 8 / (7 - 7- 0 &

21699356, 2024, 8, Downloaded from https://agupubs.onlinelibrary.wiley.com/doi/10.1029/2023JB028606 by University Of Minnesota Lib, Wiley Online Library on [13/11/2024]. See the Terms and Conditions (https://onlinelibrary.wiley.com/terms-and-conditions) on Wiley Online Library for rules of use; OA articles are governed by the applicable Creative Commons License

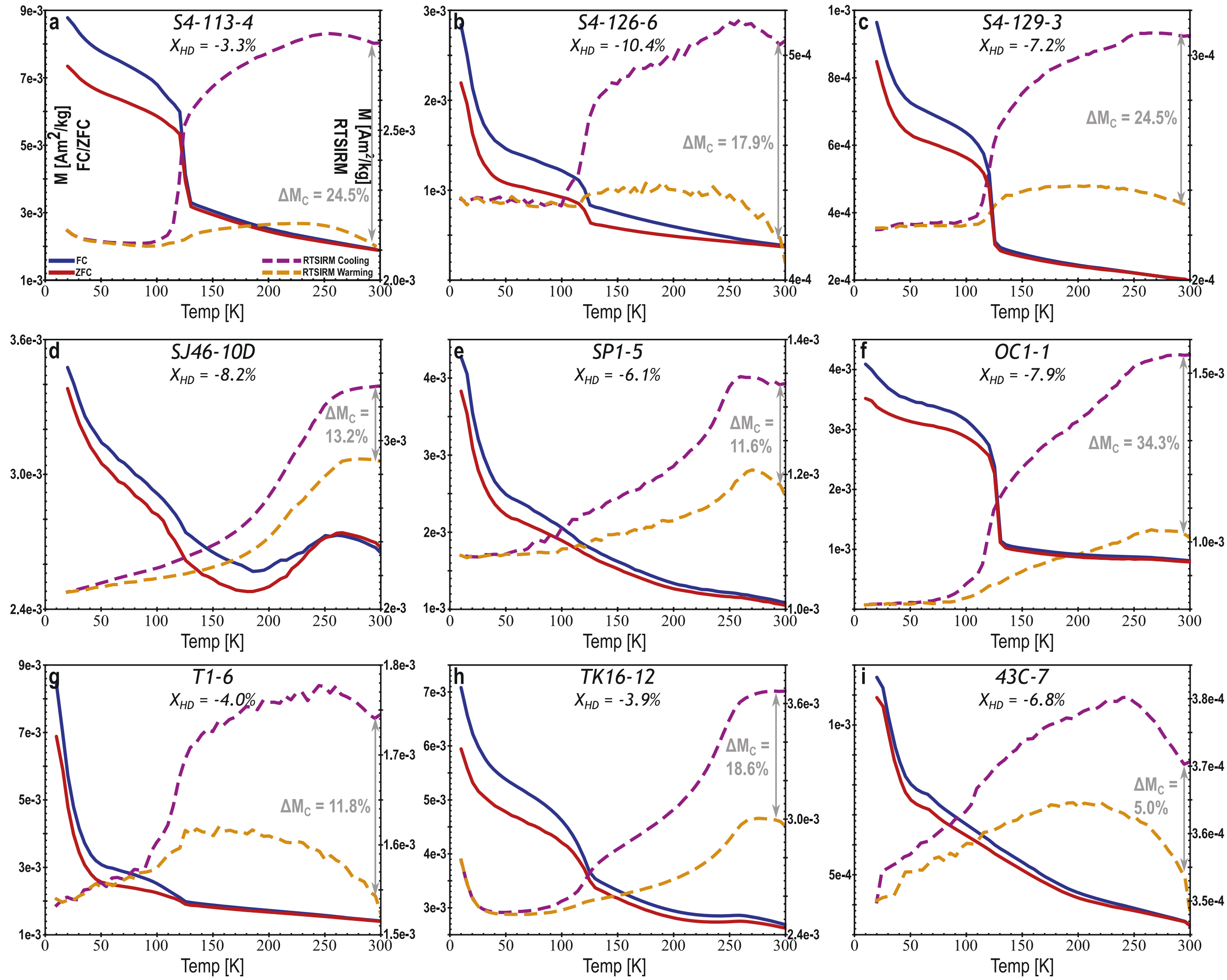

Figure 7. Low-temperature remanence curves with the range of observed behaviors. FC-ZFC (solid curves) remanence scaled to the leftward axes, LTD-RTSIRM (dashed curves) scaled to right axes. ΔM_C denotes relative loss of RTSIRM through low-temperature cycling (after Özdemir & Dunlop, 2010).

systematic relation between χ_{HD} and the presence of goethite, which is roughly quantified by the difference between FC and ZFC LTSIRM curves at 130 K, normalized by the ZFC LTSIRM at the same temperature.

3.4. High-Temperature Susceptibility and Heating Effects

All samples with negative χ_{HD} have a significant drop in susceptibility before 100°C (Figure 8). Most specimens also produce large susceptibility drops near 580°C (consistent with the Curie point of magnetite) (Figures 8a and 8b), though for several specimens this drop is small and gradual. Many samples undergo large increases above 400–450°C which then drops at 580°C (e.g., Figure 8c)—some of these are likely Hopkinson peaks for magnetite, although in many instances susceptibility is much higher after cooling from $T > 600$°C, which indicates magnetite neoformation from pre-existing minerals. Repeated cycles usually result in continued increases, and artificial magnetite growth is particularly pronounced in specimens heated in an argon atmosphere.

In many specimens, the pre-100°C susceptibility drop is almost completely recoverable when peak heating temperatures do not exceed 200–300°C. Partial recovery is possible up to 500° or so (Figures 8a and 7c). The temperature reversibility of this feature suggests an order-disorder transition with an apparent Curie point between 75.2 and 90.3°C, with an average of 83.2°C ($n = 21$, $\sigma = 3.4$), as determined by the local minimum of the temperature-derivative of susceptibility (Fabian et al., 2013; Petrovský & Kapička, 2006) (Figures 8b and 8d).

21699356, 2024, 8, Downloaded from https://agupubs.onlinelibrary.wiley.com/doi/10.1029/2023JB028606 by University Of Minnesota Lib, Wiley Online Library on [13/11/2024]. See the Terms and Conditions (https://onlinelibrary.wiley.com/terms-and-conditions) on Wiley Online Library for rules of use; OA articles are governed by the applicable Creative Commons License

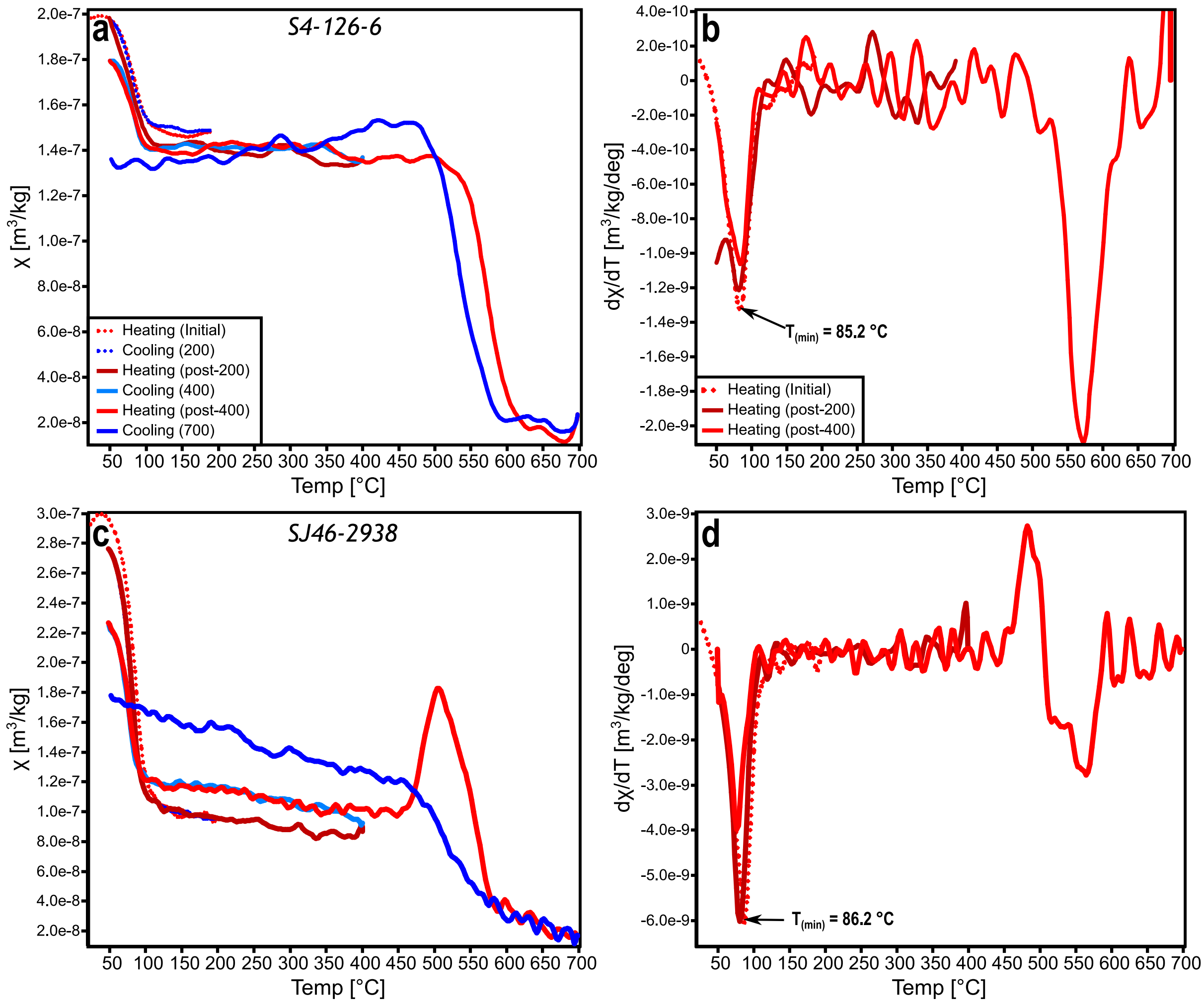

8 &7 7 & ' / 0))) & /') 0 & 8 (/ ' 0) G 5B (- /) 0 5

& & 1) & 5 ' ') & @ &) . &' 8) ' : ' &) & ' / M0) 2M3N2M 1 & 8 5 & & ' 1 &) &)) 8 / 25 - 0 &) 7)) & &7 /- 23N22 # 0)) & 9 7)) 5 & 8) : ' & 1 1 & & &) ' 1)) ' ' & ' K 1)) ' &)) & ' & 5

& # & ; # & & / 9 E) AA KG 5 22- 0K& 1 & & ' 1 &)) ' &) ' 1 : #) X: # G 2) 8) & @ 8 1 & & & 5: & &) 8 & / 2 N 4 & 5 2 0) ' & 1 7) @ ' / - 4 05 & ') (7 -7- /: N 0 1 & & &) / NM0 ' 1 & : #) & X: # G 2 5 #) & %) & / (; 2) 4 0 &) ' @ 1 X: #) : # G) AF ' 1 &) 5 & &

21699356, 2024, 8, Downloaded from https://agupubs.onlinelibrary.wiley.com/doi/10.1029/2023JB028606 by University Of Minnesota Lib, Wiley Online Library on [13/11/2024]. See the Terms and Conditions (https://onlinelibrary.wiley.com/terms-and-conditions) on Wiley Online Library for rules of use; OA articles are governed by the applicable Creative Commons License

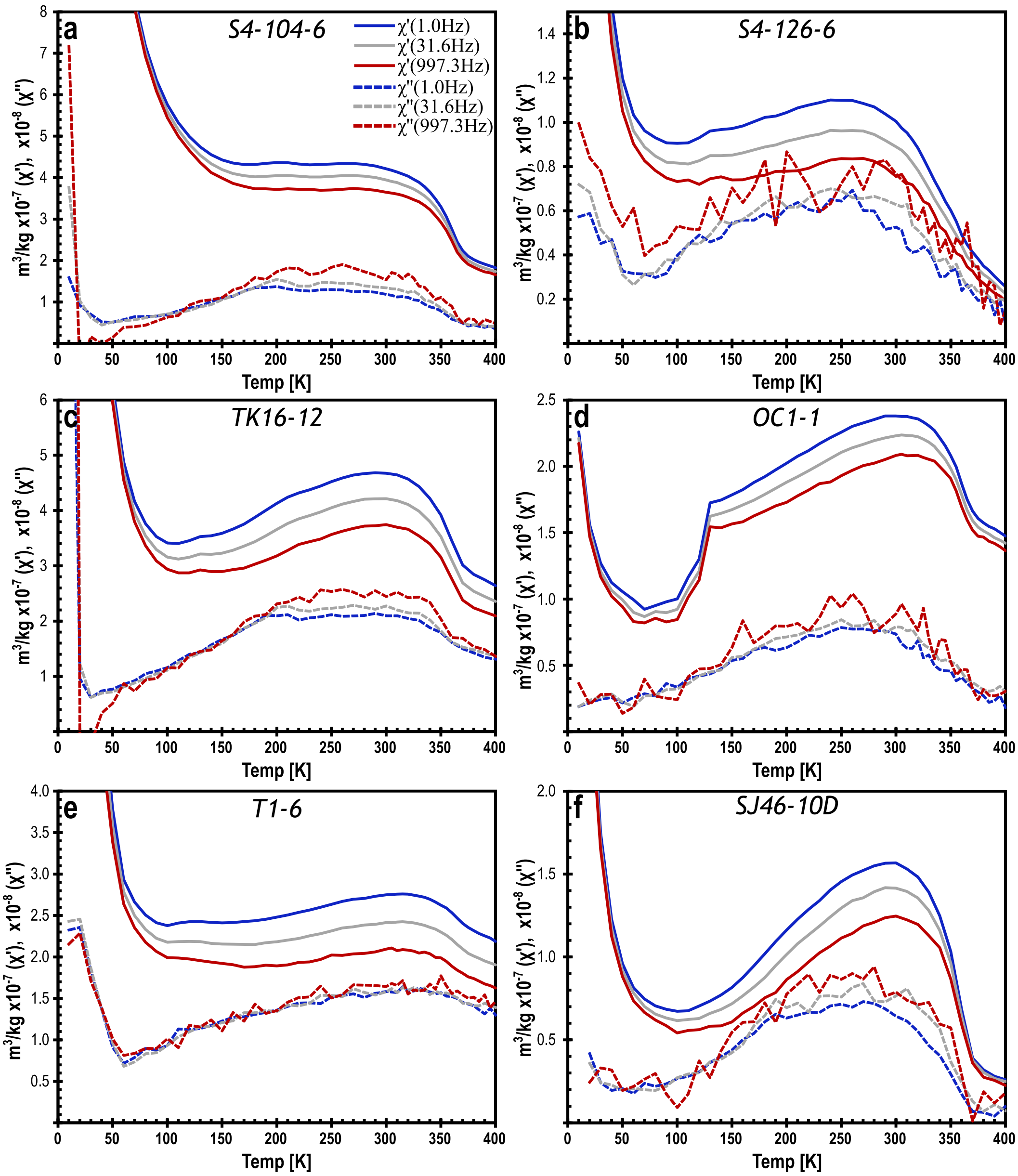

)) 7 & /O0) 7 7 & /O0 # ' & 9 2
(22 / - N#05 & ' & ' &) 9 7))
) ' & 7 &) 7 7 & ' 2 /NN#05 7 &) 7 7
&))) / 7&) . 05

1 7) ' & 1) ')) & & 7)
5

, 2

' & 9 7))) & ' ' 1
N2 / 2 #0) /: A05) & 1
' & 22 / N #0) & 1 & @
1 & ' 1 A2) / N) (#05 &
2 / (#0 ' /: A' 3A) 05 @
1 & & & , 1) & #7

21699356, 2024, 8, Downloaded from https://agupubs.onlinelibrary.wiley.com/doi/10.1029/2023JB028606 by University Of Minnesota Lib, Wiley Online Library on [13/11/2024]. See the Terms and Conditions (https://onlinelibrary.wiley.com/terms-and-conditions) on Wiley Online Library for rules of use; OA articles are governed by the applicable Creative Commons License

21699356, 2024, 8, Downloaded from https://agupubs.onlinelibrary.wiley.com/doi/10.1029/2023JB028606 by University Of Minnesota Lib, Wiley Online Library on [13/11/2024]. See the Terms and Conditions (https://onlinelibrary.wiley.com/terms-and-conditions) on Wiley Online Library for rules of use; OA articles are governed by the applicable Creative Commons License

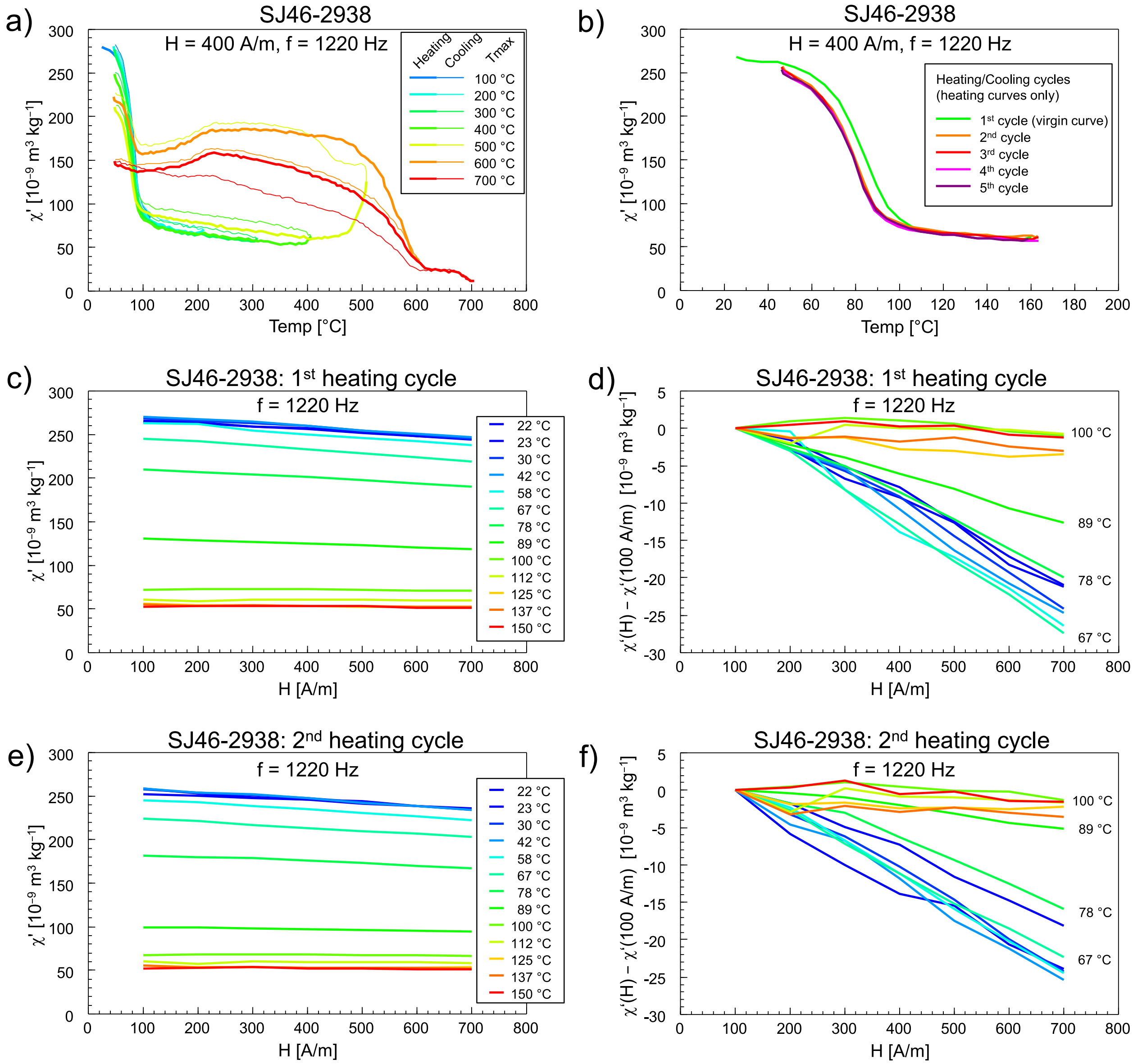

/ 0) 7 %) 7 & ' O) / (22 4 0) 9
/ 2 8 %0) 1 & & & 1) .) . 5 &&) & 1 5/' 0 / 0
2 # 5:) & & 1 5/ 0O 8 & B -7 A ; / & 0 5
/)0 / 0 % ' O 22 4 5) ')5 / 0) / 0 & / 0) /)0 &) & 5

&) ' ')) /: '05 1 : 7 .) K
1))5)) &) 5 ' : 7 .)
&) /:))05
& % & 1 & & &) / 5 5 U7)
0)5

1) B -7 A ; 1) 7 Y ' &
/: 05 &) ')) 9 ' .) & &
1 & 1) ' ' & 1 & && 1 & &) &)4 4
5 & 1 7 ' & & &

21699356, 2024, 8, Downloaded from https://agupubs.onlinelibrary.wiley.com/doi/10.1029/2023JB028606 by University Of Minnesota Lib, Wiley Online Library on [13/11/2024]. See the Terms and Conditions (https://onlinelibrary.wiley.com/terms-and-conditions) on Wiley Online Library for rules of use; OA articles are governed by the applicable Creative Commons License

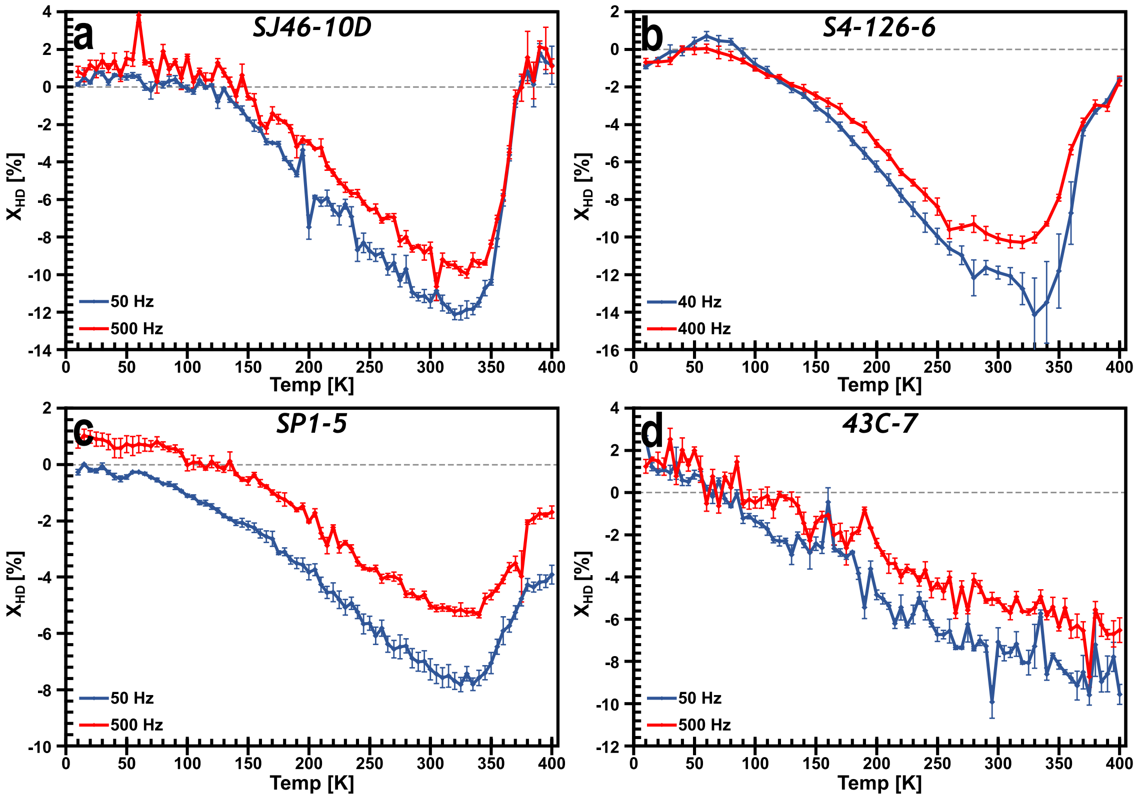

Q 5Q) ') ') NA5 N - 5 4 / 3A 0 &)
9) Q .) NA5 4 5

/: 0 ' .)) F (2F &)) . 2M 1 7
' & % 1 & & 1)) ' &
Y ' : 5

0

' / 0 &) & 223N22 4
& & . ' & & 7 &) 7 7 & ' & &)
& 1 &) &5 &)) ' & 7 &)
7 7 & ') & &)) / (5NM 7 &
22 N22 4 (7 - 0 1 & & &
/: ( ) (' 05:) 7))) ' ' /8) 22A0&
. & ' /: (05 &)) 1 &)
&) & 7 &) & . & &) 7
))) & & & ') : @
& ' 5

•

) &) & & &
) &) 222 4 / 05 & & & &) 1 7
& 5 & & & ')) & 1 &
)) &)) ') &)
& 5Q) 1 & & 5 & &
&) : 1 & & & 1 7)
& 5

21699356, 2024, 8, Downloaded from https://agupubs.onlinelibrary.wiley.com/doi/10.1029/2023JB028606 by University Of Minnesota Lib, Wiley Online Library on [13/11/2024]. See the Terms and Conditions (https://onlinelibrary.wiley.com/terms-and-conditions) on Wiley Online Library for rules of use; OA articles are governed by the applicable Creative Commons License

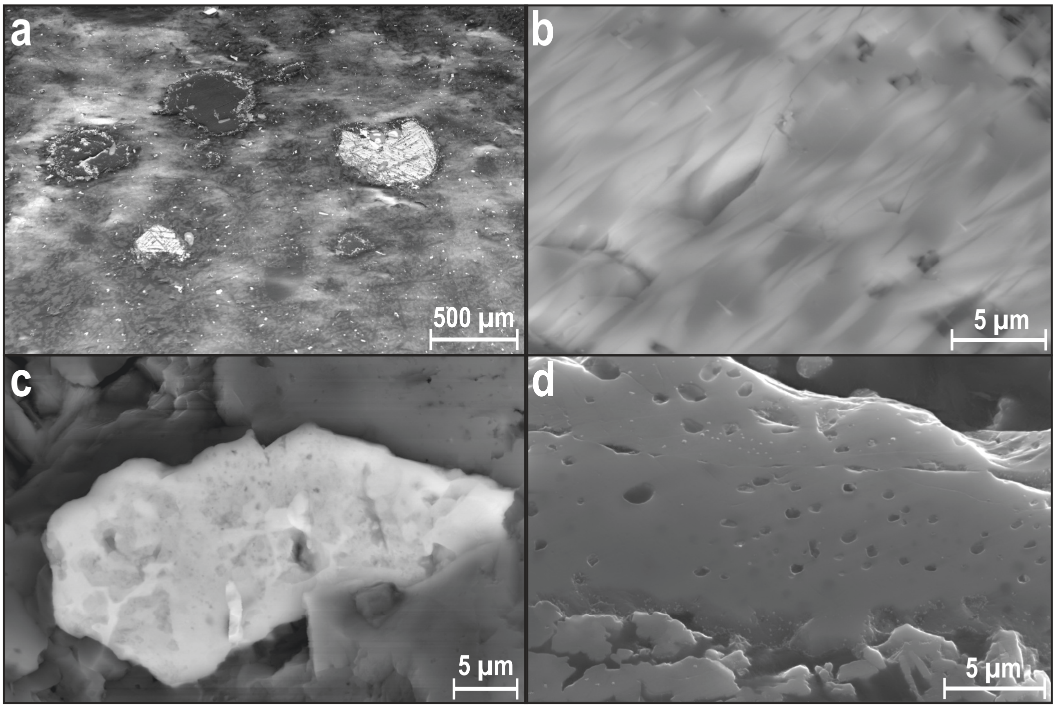

Figure 12. Scanning electron microscopy of Fe-Ti oxides in a subsample of SJ46-2938. (a) Larger view of exsolved oxides as well as those present near chlorite and dispersed in the groundmass. Bright features are Fe-oxides, large dark areas are chlorite. Some apparent brightness is due to sample charging. (b) Fine-scale Fe_2O_3 (brighter) and TiO_2 (darker) intergrowths, with bright acicular inclusions inferred to be baddeleyite (ZrO_2). (c, d) Sub-micron apparent porosity in Fe_2O_3.

It is tempting from these considerations to conclude that the observed negative χ_{HD} is the consequence of the coercivity suppressing effect produced by thermal activations in highly viscous magnetic particles, as seen with micromagnetic simulations (Lanci & Kent, 2018). It is, however, easy to show that this is not the case, by forward modeling the Rayleigh loops of thermally activated Stoner-Wohlfarth particles. The total energy E of a Stoner-Wohlfarth particle with magnetic moment m and anisotropy or microcoercivity field H_a is given by:

$$F(\theta, \psi) = \frac{E}{2\mu_0 m H_a} = \sin^2\theta - 2h(\sin\theta\cos\psi\sin\varphi + \cos\theta\cos\varphi)$$

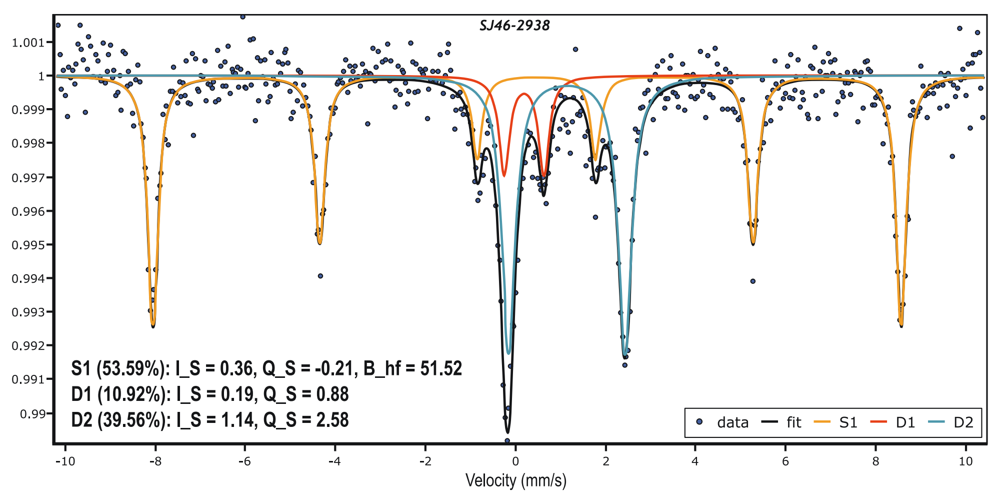

Figure 13. Room-temperature Mössbauer spectrum of sample split from SJ46-2938 along with modeled sextet and doublet components.

21699356, 2024, 8, Downloaded from https://agupubs.onlinelibrary.wiley.com/doi/10.1029/2023JB028606 by University Of Minnesota Lib, Wiley Online Library on [13/11/2024]. See the Terms and Conditions (https://onlinelibrary.wiley.com/terms-and-conditions) on Wiley Online Library for rules of use; OA articles are governed by the applicable Creative Commons License

10.1029/2023JB028606

21699356, 2024, 8, Downloaded from https://agupubs.onlinelibrary.wiley.com/doi/10.1029/2023JB028606 by University Of Minnesota Lib, Wiley Online Library on [13/11/2024]. See the Terms and Conditions (https://onlinelibrary.wiley.com/terms-and-conditions) on Wiley Online Library for rules of use; OA articles are governed by the applicable Creative Commons License

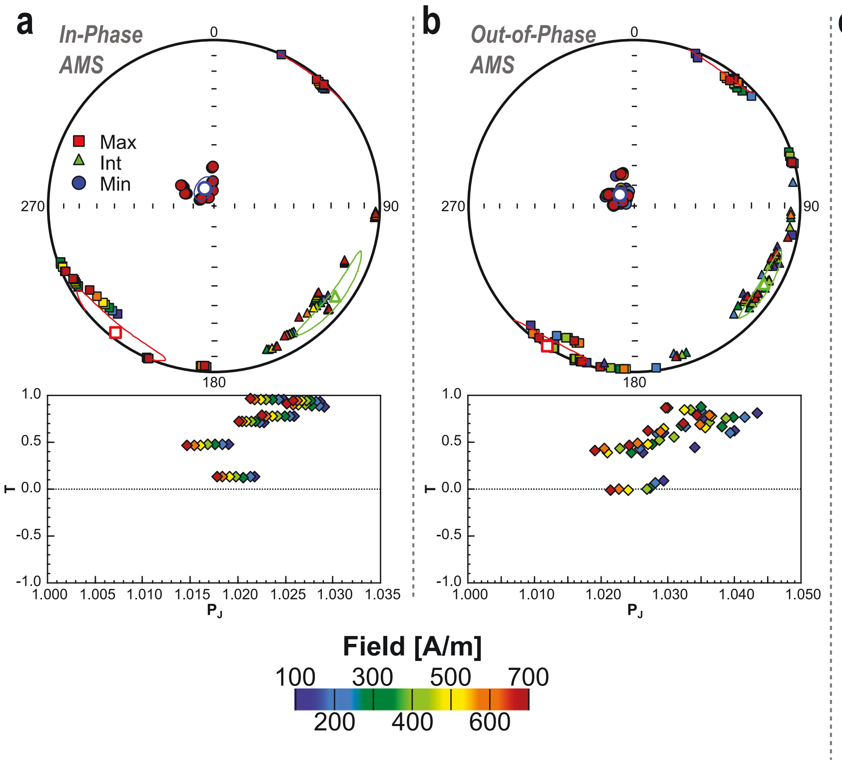

Figure 14. Field-dependence of anisotropy of magnetic susceptibility for specimens from sample S4-116. (a) Equal area and Jelinek plots for anisotropy of in-phase magnetic susceptibility. (b) Equal area and Jelinek plots for anisotropy of out-of-phase magnetic susceptibility. (c) Equal area plots of field-dependent components of in-phase and out-of-phase susceptibility tensors calculated via tensor subtraction.

where θ and ψ are the polar and azimuthal angles of the magnetic moment vector, φ is the angle between the particle easy axis and the applied field H, and $h = H/H_a$ (Stoner & Wohlfarth, 1948). In small field amplitudes $|h| \ll 1$, F has two energy minima that define the equilibrium orientations $\psi = 0$ and $\theta_1 = h \sin \varphi/(1 + h \cos \varphi)$, $\theta_2 = \pi - h \sin \varphi/(1 - h \cos \varphi)$ for the magnetic moment parallel and antiparallel to the easy axis, respectively. The two minima are separated by an energy barrier given by $\Delta E_0 = \mu_0 m H_a/2$ in $H = 0$. In small fields, one of the energy minima is deepened while the other becomes shallower, yielding two slightly different energy barriers:

$$\Delta E_{1,2} \approx 2\mu_0 m H_a (1 - 2h(\cos \psi \sin \varphi \mp \cos \varphi)).$$

These energy barriers define the transition rates $\lambda_{1,2} = \nu_0 \exp(-\beta_{1,2})$ between the equilibrium magnetizations $M_{1,2} \propto m \cos \theta_{1,2}$ measured along the applied field direction, with $\nu_0 \approx 10$ GHz being the attempt frequency and $\beta_{1,2} = \Delta E_{1,2}/k_B T$ at the absolute temperature T. The magnetic response to a small oscillating field is thus given by the solution of the differential equation

$$\dot{p}_1 = \lambda_2 (1 - p_1) - \lambda_1 p_1$$

for the occupation probability p_1 of the energy minimum 1. Figure 15 is an example of viscous Rayleigh loops obtained by the solution of the above equations for $\varphi = 45°$. The energy barrier ΔE_0 has been chosen so, that the saturation effect is maximized. This occurs when viscosity is maximized as well. Other particle orientations give similar results, with the low-field susceptibility $|\chi_1|$, defined by the Fourier series expansion

$$M(t) = H_{max} \sum_{k=1}^{\infty} (\chi')_k \cos k\omega t + (\chi'')_k \sin \omega t$$

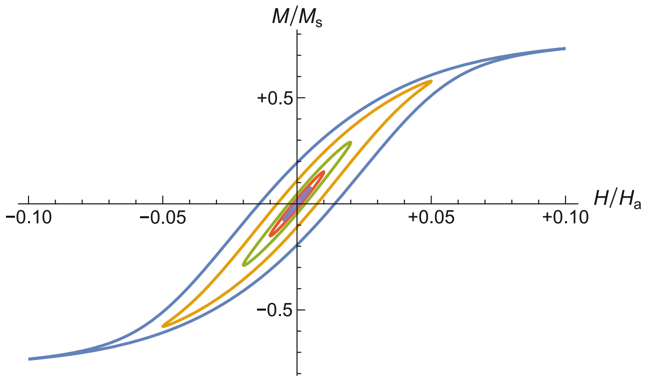

Figure 15. Simulated Rayleigh loops for Stoner-Wohlfarth particles with easy axis at 45° to the applied field, zero-field energy barrier $\Delta E_0 = 15$kBT, in a 976 Hz sinusoidal field with $H_{max}/H_a = 0.005$, 0.01, 0.02, 0.05, and 0.1.

decreasing significantly only for $H_{max}/H_a > 0.05$. Taking $H_{max} = 700$ A/m as for the definition of χ_{HD}, this condition translates into anisotropy fields $\mu_0 H_a < 18$ mT, which is significantly smaller than the minimum anisotropy field $\mu_0 H_a = 4|K_1|/3M_s \approx 37.5$ mT of magnetite particles dictated by its magnetocrystalline anisotropy constant K_1, and orders of magnitude smaller than the anisotropy field of high-coercivity minerals such as hematite. Maghemite (Birks, 1950; Takei & Chiba, 1966) has a lower magneto-crystalline anisotropy constant ($|K_1| = 4.7$ kJ/m^3 compared to 13.5 kJ/m^3 for magnetite) which, would yield $\mu_0 H_a \approx 16$ mT for perfectly isometric particles. However, maghemite is not a primary mineral in rocks, and forms by low-temperature oxidation of magnetite through diffusive loss of Fe(II). The internal stress resulting from this process (Yuan et al., 2019) increases the coercivity of the affected magnetite particles, and thus the associated anisotropy field, relative to the parent magnetite (Cui et al., 1994; Van Velzen & Zijderveld, 1992).

Forward calculations of the AC magnetic susceptibility behavior of thermally-activated particles also show major differences from the behaviors observed. The equilibrium magnetization of randomly-oriented, thermally-activated particles of volume V in an applied field H_{app} is governed by the Langevin equation: $M_{eq} = M_s\left(\coth(\alpha) - \frac{1}{\alpha}\right)$ where $\alpha = \frac{\mu_0 V M_s H_{app}}{k_b T}$. This results in a maximum susceptibility at $H_{app} = 0$, though the decrease is negligible at fields less than a few thousand A/m for M_s values of known magnetic minerals.

The in-phase AC susceptibility at angular frequency ω is given by $\chi' = \frac{M_{eq}}{H_{app}(1+\omega^2\tau^2)}$ and the out-of-phase susceptibility by $\chi'' = \chi'\omega\tau$. The expected χ_{HD} can then be calculated using the full field-dependent relaxation time relation $\tau = \tau_0 e^{\left[\frac{VK}{k_b T}\left(1-\frac{H_{app}}{H_K}\right)^2\right]}$, with the simplification that the effective anisotropy constant $K = \frac{\mu_0 M_s H_K}{2}$, where H_K is the microscopic coercivity.

Preliminary models of field-dependence of magnetic susceptibility were constructed using these equations for magnetite ($M_s = 480{,}000$ A/m) at a range of H_K values (Figure 16). Varying M_s in this model does not affect the absolute range of χ_{HD} at a specified H_K—altering the value of M_s results in the same maximum and minimum values while only shifting the particle sizes at which these occur. The maxima and minima are only sensitive to measuring frequency and H_K. The high and low frequencies of the MFK-1 Kappabridge (976 and 15616 Hz) were used for comparison to actual data.

At the smallest particle sizes, χ_{HD} is weakly negative and becomes increasingly negative until it approaches approximately 70% of the blocking volume, at which point it rapidly becomes positive as higher field amplitudes allow for more relaxation. For values of H_K consistent with magnetite (≥37.5 mT), minimum χ_{HD} is

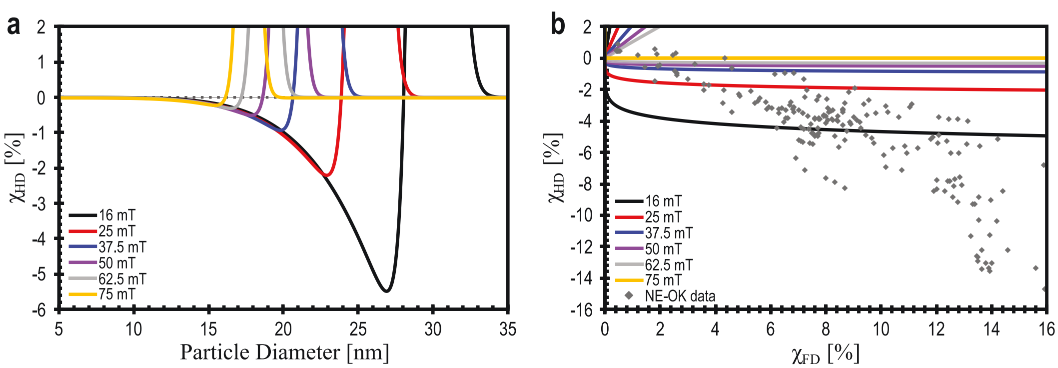

Figure 16. Models of field-dependent susceptibility of thermally-activated superparamagnetic particles. (a) Field-dependence versus particle diameter models for a range of microcoercivity values. (b) Field-dependence versus frequency-dependence for modeled particles (curves) compared to measured values of northeastern Oklahoma specimens.

21699356, 2024, 8, Downloaded from https://agupubs.onlinelibrary.wiley.com/doi/10.1029/2023JB028606 by University Of Minnesota Lib, Wiley Online Library on [13/11/2024]. See the Terms and Conditions (https://onlinelibrary.wiley.com/terms-and-conditions) on Wiley Online Library for rules of use; OA articles are governed by the applicable Creative Commons License

21699356, 2024, 8, Downloaded from https://agupubs.onlinelibrary.wiley.com/doi/10.1029/2023JB028606 by University Of Minnesota Lib, Wiley Online Library on [13/11/2024]. See the Terms and Conditions (https://onlinelibrary.wiley.com/terms-and-conditions) on Wiley Online Library for rules of use; OA articles are governed by the applicable Creative Commons License

21699356, 2024, 8, Downloaded from https://agupubs.onlinelibrary.wiley.com/doi/10.1029/2023JB028606 by University Of Minnesota Lib, Wiley Online Library on [13/11/2024]. See the Terms and Conditions (https://onlinelibrary.wiley.com/terms-and-conditions) on Wiley Online Library for rules of use; OA articles are governed by the applicable Creative Commons License

21699356, 2024, 8, Downloaded from https://agupubs.onlinelibrary.wiley.com/doi/10.1029/2023JB028606 by University Of Minnesota Lib, Wiley Online Library on [13/11/2024]. See the Terms and Conditions (https://onlinelibrary.wiley.com/terms-and-conditions) on Wiley Online Library for rules of use; OA articles are governed by the applicable Creative Commons License

21699356, 2024, 8, Downloaded from https://agupubs.onlinelibrary.wiley.com/doi/10.1029/2023JB028606 by University Of Minnesota Lib, Wiley Online Library on [13/11/2024]. See the Terms and Conditions (https://onlinelibrary.wiley.com/terms-and-conditions) on Wiley Online Library for rules of use; OA articles are governed by the applicable Creative Commons License

' 5 8 5B5 6 5 5 E 8 5 5/ 22 05G & & 3 .
% 5F B/- ; AN0 N3 25& F44) 5 4 25 2 ; 4 22A(
5, 5 E) B5 5/ 222 05G 1 7) / ; 2 # 0F
& %)) 5 / N0 - (N3 - (N 5& F44) 5 4 25 2 A4
222B A22 (2
6 5# 5 E & & 6 5 5/ A(; 05 & & & 5)
M) /; - 0 AA3- (5& F44) 5 4 25 2A; 4 5 A(; 5222N
8 5 E # &' 5/ A- - 05,) . 7 1 j 7: 5) /N0
3 - 5& F44) 5 4 25 (4B B5 5
. G5) 5 5 5 E 5/ AA- 05 ' 1 71) & 5
/ 0 N 3 ; 5& F44) 5 4 25 2 A4A B 2 2(
, & # 5 E 5/ 22 05 &))) # ' &)
' & 8 7 ' 8 1 5) B/ 3 0 23 A5& F44) 5 4 25 2 - 45 5 22 52N52 2
, , % 5B5 E X B)) B5 5 5/ AA 05 &))) &) %)
7) / ' 05 C / 0 NA3A25& F44) 5 4 25 45 - 7 (- U5
AA 5' 22N 5
8 5 5/ AA 05) ') 1))))) % & 5)
) C / 3 0 3 ; 5& F44) 5 4 25 2 - 422 7A 2 /A 0A2 N7
8 5 5/ AA; 05 & Z ')) 9)) ' 5
C / 0 2 3 2- 5& F44) 5 4 25 2(- 45 - 7 (- U5 AA; 5 (- ; 5
Q 5 G 5 5 # & 5) 5 8 5 ') 5 5/ 2 A05 .))))) 5F
/ 0 N2 5& F44) 5 4 25 2 ; 4 ((- N72 A72; (N272

21699356, 2024, 8, Downloaded from https://agupubs.onlinelibrary.wiley.com/doi/10.1029/2023JB028606 by University Of Minnesota Lib, Wiley Online Library on [13/11/2024]. See the Terms and Conditions (https://onlinelibrary.wiley.com/terms-and-conditions) on Wiley Online Library for rules of use; OA articles are governed by the applicable Creative Commons License